iScience

CellPress
OPEN ACCESS

Article

Identifying new players in structural synaptic plasticity through *dArc1* interrogation

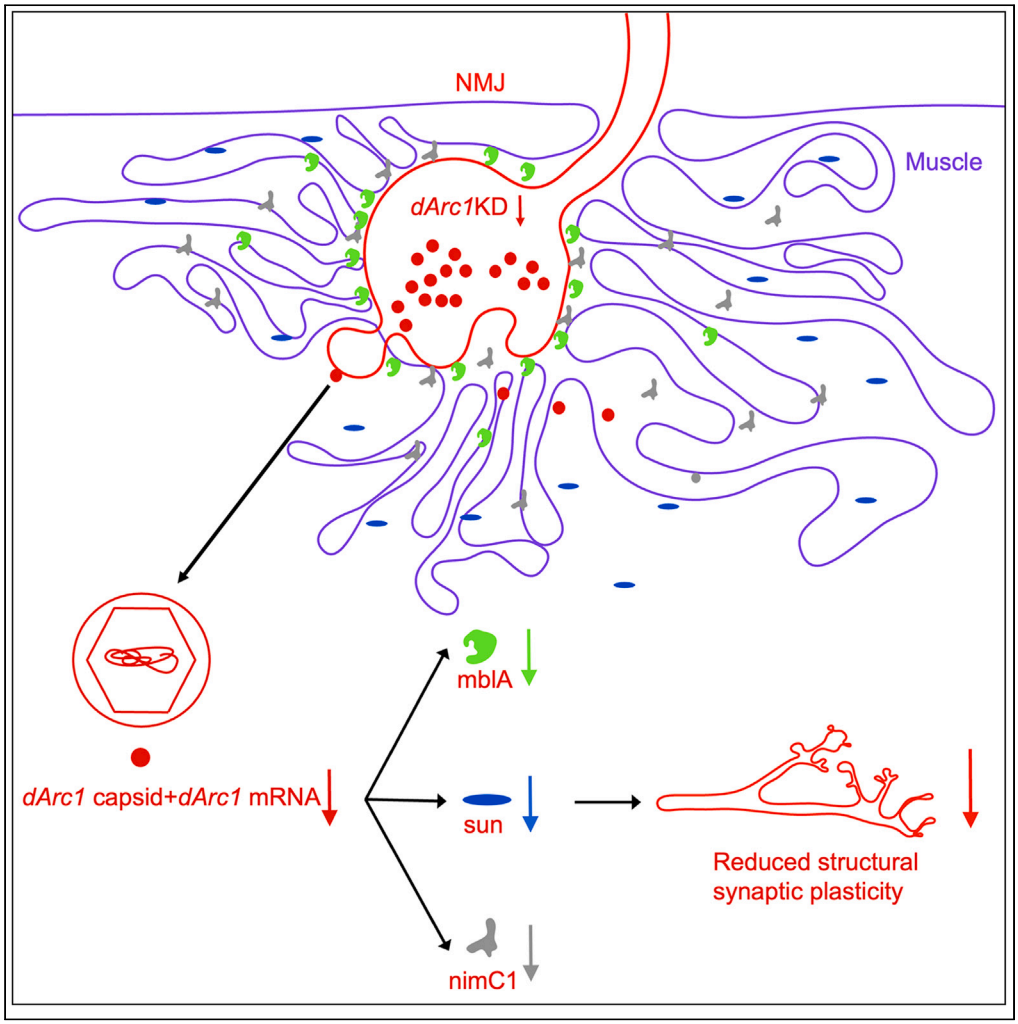

Cong Xiao, P. Githure M'Angale, Shuhao Wang, Adrienne Lemieux, Travis Thomson

travis.thomson@umassmed.edu

Highlights

Used the powerful genetics of *Drosophila* to identify genes that regulate plasticity

Drosophila Arc (dArc1) regulates plasticity through several distinct pathways

Repression of dArc1 affects mRNAs pre- and postsynaptically

Identification of potential mRNA cargo of dArc1 capsids

Xiao et al., iScience *26*, 108048
November 17, 2023
https://doi.org/10.1016/j.isci.2023.108048

iScience

CellPress
OPEN ACCESS

Article

Identifying new players in structural synaptic plasticity through *dArc1* interrogation

Cong Xiao,[1] P. Githure M'Angale,[1] Shuhao Wang,[1] Adrienne Lemieux,[1] and Travis Thomson[1,2,*]

SUMMARY

The formation, expansion, and pruning of synapses, known as structural synaptic plasticity, is needed for learning and memory, and perturbation of plasticity is associated with many neurological disorders and diseases. Previously, we observed that the *Drosophila* homolog of Activity-regulated cytoskeleton-associated protein (dArc1), forms a capsid-like structure, associates with its own mRNA, and is transported across synapses. We demonstrated that this transfer is needed for structural synaptic plasticity. To identify mRNAs that are modified by dArc1 in presynaptic neuron and postsynaptic muscle, we disrupted the expression of *dArc1* and performed genomic analysis with deep sequencing. We found that dArc1 affects the expression of genes involved in metabolism, phagocytosis, and RNA-splicing. Through immunoprecipitation we also identified potential mRNA cargos of dArc1 capsids. This study suggests that dArc1 acts as a master regulator of plasticity by affecting several distinct and highly conserved cellular processes.

INTRODUCTION

Structural synaptic plasticity is thought to be a key process by which learning and memory occur. It encompasses the formation, growth, or removal of synaptic connections between neurons as well as modifications in the dimensions and morphology of individual synapses.[1–3] In mammals, activity-regulated cytoskeleton-associated protein (*Arc/Arg3.1*) is an immediate-early gene that is expressed broadly at a low basal level. However, its expression can be strongly induced by intense neuronal activity and newly synthesized *Arc* RNA exhibits rapid trafficking into dendrites.[4–8] *Arc* is crucial for the structural and functional changes which occur in synapses during learning and memory processes.[9,10] During intense neuronal activity, Arc protein accumulates quickly in postsynaptic sites along with postsynaptic density (PSD) family proteins via local protein synthesis[11] and forms 1.5-MDa supercomplexes.[12] Arc controls synaptic strength bidirectionally through mediating actin cytoskeletal dynamics and AMPA-type glutamate receptor (AMPAR) trafficking in dendritic spines and axons.[13,14] A recent study reported that the N-terminal domain (NTD) motif plays a pivotal role in facilitating higher-order oligomerization, virus-like assembly, and exogenous RNA-induced oligomerization.[15]

The *Drosophila* Arc homolog (dArc1) has been found to form retrovirus-like capsids and bind to its own mRNA, and has been described as a Gag-like protein. dArc1 is involved in structural synaptic plasticity and is transported from the pre-to postsynaptic regions along with its RNA. Additionally, its domains that are similar to Gag retroelements play a crucial role in mediating cellular communications in the nervous system.[16,17] Although mammalian *Arc* and *dArc1* evolved independently in tetrapods and insect genomes,[18] they share a functional similarity. At the monomer level, dArc1 folds in a similar manner to HIV-1, Ty3, and rat Arc.[19–21] In S2 cells, stranded at second (Sas) facilitates dArc1 trafficking to distant receptor tyrosine phosphatase 10D (Ptp10D)-expressing recipient cells, which was also demonstrated *in vivo*.[22] However, it is still unclear how dArc1 regulates structural synaptic plasticity and what role its transfer plays in this process.

The motor neuron endings situated at the body wall muscles in *Drosophila* larvae comprise numerous presynaptic boutons. The regions preceding (boutons) or succeeding (subsynaptic reticulum of the muscle) this junction are referred to as pre- or post-synapse, respectively. This junction is a neuromuscular junction (NMJ), which serves as a robust model system to investigate the cellular and molecular mechanisms underlying synapse formation and adaptability.[23] To further investigate the role of dArc1 in synaptic plasticity, we employed this model and utilized the binary GAL4/UAS system to specifically downregulate *dArc1* in the neuron. We then investigated the transcriptomic changes separately in neurons and muscles (opposing sides of the NMJ) through bulk RNA-seq. As dArc1 protein and RNA are transported from pre-to postsynaptic regions[16] and mediate structural synaptic plasticity through this transfer, this allowed us to distinguish differentially expressed genes (DEGs) separately in muscles and neurons. Gene ontology (GO) analysis shows that the top pathways that DEGs are involved in are cation transport, starvation response, nutrition levels, and extracellular stimulus. We further investigated several dArc1 target genes and demonstrated that downregulation of *mbl* in either pre- or postsynaptic sites causes dramatic reductions of bouton numbers, while

[1]Department of Neurobiology, University of Massachusetts Chan Medical School, 364 Plantation Street, Worcester, MA 01605, USA
[2]Lead contact
*Correspondence: travis.thomson@umassmed.edu
https://doi.org/10.1016/j.isci.2023.108048

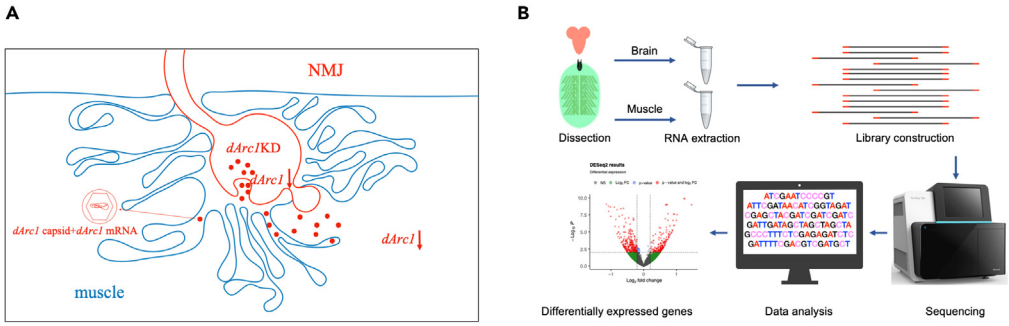

Figure 1. Schematic illustration of the fly model and experimental process to find novel genes involved in plasticity

(A) The fly model of *dArc1* knockdown in the neuron.

(B) The experimental process used in this study, including dissection of brains and muscles, extraction of RNAs, library construction, sequencing, and data analysis.

downregulation of *sun* or *nimC1* only in postsynaptic muscles, not in presynaptic neurons, results in a drastic decrease in bouton numbers. We provide evidence that dArc1 mediates structural synaptic plasticity through affecting the expression of genes involved in energy metabolism, phagocytosis, and RNA metabolic pathways.

RESULTS

dArc1 knockdown in neurons causes the reduction of *dArc1* and affects gene expression in both pre- and postsynapse

dArc1 protein forms a capsid-like structure and is transported across the synapse along with its RNA transcript, and this transfer is involved in structural synaptic plasticity.[16] As such, we hypothesized that dArc1 might mediate structural synaptic plasticity by affecting expression of genes in pre- and/or postsynapse, or even mediates the transfer of other mRNAs from nerves to muscles. To address this, we downregulated *dArc1* specifically in motor neurons using a GAL4 driver (C380-GAL4) to express UAS-*dArc1*-RNAi, and then sequenced transcriptomes in both brains (presynapse at the NMJ) and muscles (postsynapse at the NMJ) to identify DEGs affected by dArc1 (Figures 1A and 1B).

In our presynaptic neuron sequencing data, *dArc1* was reduced by 35%, with an adjusted value of p = 0.002024306 (Figures 2A and 2B; Table S1), and DEG analysis found a total of 204 downregulated and 216 upregulated genes (Table S1). The GO biological process analysis showed high neuron development-related pathways, as expected for targeting a gene involved in neuronal plasticity, and the top pathways affected were cytoplasmic translation, G protein-coupled receptor signaling pathway, and axon extension (Figure 2C).

In our postsynaptic muscle sequencing data, we found that *dArc1* showed a reduction of 54%, with an adjusted value of p = 0.0000261 (Figures 2D and 2E; Table S2). DEG analysis indicated a total of 144 downregulated and 102 upregulated genes (Table S2). The GO biological process analysis showed effects on muscle development-related pathways, with the top pathways affected being cation transmembrane transport, ion transmembrane transport, membrane transporter activity, response to nutrient level, and response to extracellular stimulus (Figure 2F).

Categorization and GO analysis

In order to obtain a more comprehensive understanding of the sequencing data, we divided the data into discrete sets of expression patterns based on the combinations of expression changes of DEGs (downregulated, -; upregulated, +; nonsignificant difference, ns) in pre- and postsynaptic regions to identify candidate genes that are regulated by dArc1 specifically in each neuron and muscle, or in both. Our logic in doing this was to find the potential cargos of dArc1 capsids that are context-specific or ubiquitous (Table 1). Subsequently, we conducted GO analysis on these six patterns individually (Table S3), which revealed promising pathways associated with pattern 2 (genes that show no significant difference in the presynaptic region and are downregulated in the postsynaptic region; ns/-) and pattern 6 (upregulated in the presynaptic region and showing no significant difference in the postsynaptic region; +/ns). Biological process analysis shows that in pattern 2 (ns/-), the set of DEGs was primarily involved in transmembrane transport, responses to nutrient levels and extracellular stimuli, and negative regulation of TOR signaling, which includes genes known to be implicated in cancer, neurodegenerative diseases, and metabolic disorders (Figure 3A). Cellular component analysis indicated that these genes are predominantly located on the mitochondrial membrane or organelle envelope (Figure 3B) and molecular function analysis revealed that they are mostly involved in cation/ion/inorganic/proton transmembrane transporter activity and symporter activity (Figure 3C). In contrast, pattern 6 (+/ns) DEGs are predominantly associated with locomotion, axonogenesis, synapse organization, axon guidance, and eye photoreceptor cell development in biological process analysis (Figure 3D). Cellular component analysis revealed these genes are mainly expressed in cell junctions, neuron projections, synapses, axons, and presynaptic regions (Figure 3E). Molecular function analysis suggested that they mainly function in enzyme regulator activity, GTPase regulator activity, and cell adhesion molecule binding (Figure 3F).

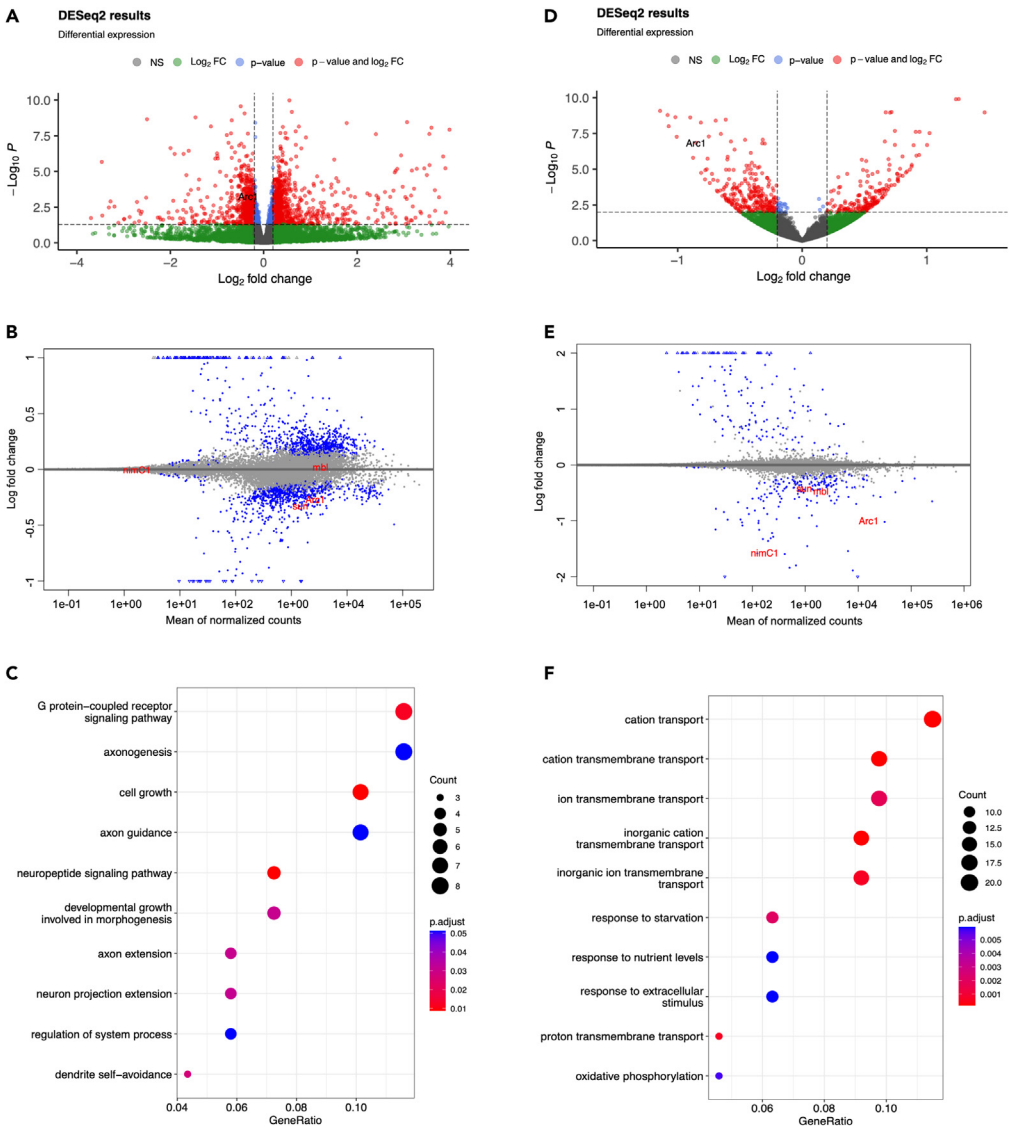

Figure 2. RNA-seq data analysis

(A) Volcano plot of RNA-Seq data in the neuron, where the x axis represents fold change in transcripts from muscle when *dArc1*RNAi-neuron versus control (a positive score represents enrichment, a negative score represents depletion). The y axis represents statistical confidence for each x axis point. dArc1 is marked.

(B) MA plot of RNA-seq data, where the x axis represents statistical confidence for each y axis point. The y axis represents fold change in transcripts from muscle when *dArc1*RNAi-neuron versus control.

(C) GO biological process analysis of the differentially expressed genes.

(D) Volcano plot of RNA-Seq data in the muscle, where the x axis represents fold change in transcripts from muscle when *dArc1*RNAi-neuron versus control (a positive score represents enrichment, a negative score represents depletion). The y axis represents statistical confidence for each x axis point. dArc1 is marked.

(E) MA plot of RNA-seq data, where the x axis represents statistical confidence for each y axis point. The y axis represents fold change in transcripts from muscle when *dArc1*RNAi-neuron versus control.

(F) GO biological process analysis of the differentially expressed genes.

Among the DEGs in patterns 1 (−/−), 3 (-/ns), 4 (+/+), and 5 (ns/+), the results of the biological process and molecular function analysis indicate that only pattern 3 (-/ns) contained genes involved in neuropeptide signaling pathways. This included neuropeptide receptor binding, neuropeptide hormone activity, and G protein-coupled receptor binding according to molecular function analysis (Figure S1A). Pattern 1 (1/-) was primarily linked to oxidative phosphorylation, respiration, and metabolism (Figure S1B), while pattern 4 (+/+) was primarily associated with misfolded protein binding, heat shock protein binding, and ATP-dependent protein folding chaperone (Figure S1C). Interestingly, no specific pathways were identified for pattern 5 (ns/+).

Table 1. The patterns of differentially expressed genes

Pattern	Presynapse	Postsynapse	Represented genes
1	–	–	*dArc1, sun, Cyp12c1, GstE1, ox, CG30054*
2	ns	–	*mbl, nimC1, nimB1, mthl3, mthl4*
3	–	ns	*GstE2, GstE3, Cpr51A, Cyp9h1, Fmrf, RpL21, RpL29, RpLP1, Fer2,*
4	+	+	*mthl8, Cyp4p1, Cyp4p2, ppk11, ppk16, Hsp70Bb, Hsp70Bbb, eIF4E-3*
5	ns	+	*ppk11, ppk16, ppk13, Ptr, GstE9,*
6	+	ns	*mthl6, mthl2, nimC3, eater, nimB4, nimA*

Identification of *mbl*, *sun*, and *nimC1* in RNA-seq data

The RNA-seq data obtained from the postsynaptic muscle identified *mbl* as a significantly downregulated gene (Figures 2E and S2 A2). The sequence of *mbl* is more than 150 kb pairs in the *Drosophila* genome with 18 isoforms. It encodes an RNA binding protein involved in RNA metabolism through alternative splicing, targeting mRNA localization, and circRNA biogenesis.[24–26] It was first found to be a suppressor of the *sev-svp2* eye phenotype[27] in flies. In a *Drosophila* myotonic dystrophy model, *mbl* is mislocalized in the muscle sarcomere.[28] Its mammalian homolog, muscleblind-like (MBNL), is involved in neuromuscular disorders such as myotonic dystrophy type1 (DM1), and sustainable recovery of MBNL activity in an autoregulatory feedback loop shows some benefits in cells derived from patients with DM1.[29,30] *MBNL* has three isoforms with distinct functions.[31] Notably, the expression of *mbl* was not changed in the presynaptic neuron (pattern 2) RNA-seq data (Figures 2B and S2 A2; Table S1).

We found numerous DEGs involved in metabolism, including members of the *Methuselah-like* protein family, such as *mthl3, mthl4, mthl8,* and the methuselah ligand *sun* (Figures 2E and S2 B3; Table S2). Many of these genes are involved in responses to starvation, nutrient levels, and extracellular stimulus pathways. *Methuselah* family proteins typically are in the Class B secretin family of G-protein-coupled receptors involved in life span which function in presynaptic regions to increase neurotransmitter exocytosis at the NMJ, but *mthl3, mthl4,* and *mthl8* do not have clearly defined biological functions.[32,33] *Methuselah* family genes and the ligand *sun* together manipulate organ growth by modifying brain *Drosophila* insulin-like peptides (Dilps) secretion.[34] In our presynaptic neuron RNA-seq data, the expression of *sun* was significantly decreased (Figures 2B and S2 A3; Table S1).

We identified members of the *nimrod* gene superfamily in our set of DEGs, including *nimC1* and *nimB1* (Figures 2E and S2 B4; Table S2). *nimC1* encodes a 90-kDa transmembrane protein possessing ten NIM repeats within its extracellular region, a single transmembrane domain, and a short cytosolic tail. *nimC1* is involved in bacterial phagocytosis and plays a pivotal role in the uptake of latex beads and zymosan particles. Suppression or overexpression of *nimC1* leads to enhanced or weakened phagocytosis, respectively.[35,36] We found that the expression of *nimC1* was extremely low and did not change in the presynaptic neuron RNA-seq data after neuronal disruption of *dArc1* (Figures 2B and S2 A4; Table S1), but was downregulated in the postsynaptic muscle.

We also noted several genes that might be involved in synaptic plasticity. *ox* encodes a protein which is involved in mitochondrial biogenesis and can alter nuclear gene expression,[37] and we found that it was dramatically decreased in both neurons (39%) and muscles (35%). *Kazl-ORFB* (decreased 40% in the muscle) is located in the extracellular region and mitochondrion, and has been predicted to mediate serine-type endopeptidase inhibitor activity by the Alliance of Genome Resources, a consortium of seven model organism databases (MODs) and the Gene Ontology (GO) Consortium (referred to as Alliance). It was also found to be drastically decreased in both muscles and neurons in our data. The functions of *CG9338* (reduced 35% in the muscle) are not clear, but it is predicted to play a role in the regulation of cholinergic synaptic transmission, positive regulation of voltage-gated potassium channel activity, and sleep by Alliance. *Cyp12e1* (expression reduced by 37% in the muscle) is predicted by Alliance to be involved in several functions, including iron ion binding activity, heme binding activity, and monooxygenase activity. *DOR* (expression reduced by 54% in the muscle) is crucial for endosomal sorting and promotes the trafficking of vesicles to lysosomes for degradation at the NMJ.[38] (Tables S1 and S2)

Validation of dArc1 target genes by RT-qPCR

To validate the DEGs in the muscle, we again utilized the motor neuron-specific GAL4 driver C380-GAL4 to express UAS-*dArc1*-RNAi to specifically downregulate *dArc1* in the neuron, and then separately isolated muscle and neuron tissues. *dArc1* showed drastic decreases in both neurons and muscles, with expression decreased by 65% and 70%, respectively (Figures 4A and 4B). We validated several of the DEGs found in our RNA-seq data, including *nimC1, sun, mbl, ox, CG9338,* and *Cyp12e1*. Consistent with our sequencing data, we found *nimC1* showed a significant decrease in expression of more than 60% in the muscle but was below the detection threshold in the neuron (Figures 4A and 4B). This was expected because *nimC1* encodes a transmembrane protein which is located primarily in phagocytic cells in the hemolymph. The expression levels of *mbl*, *sun*, *ox*, *CG9338*, and *Cyp12e1* showed significant reductions in the muscle tissue after disruption of *dArc1* in neurons (Figure 4A) but were not changed in the neuron (Figure 4B). Additionally, we assessed the expression levels of several genes in the muscle, such as *Kaz1-ORFB*, *CG17508*, *Ptr*, *DOR*, and the long non-coding RNA *CR43417*. However, only *Kaz1-ORFB* showed results that were consistent with the sequencing data (Figure 4A).

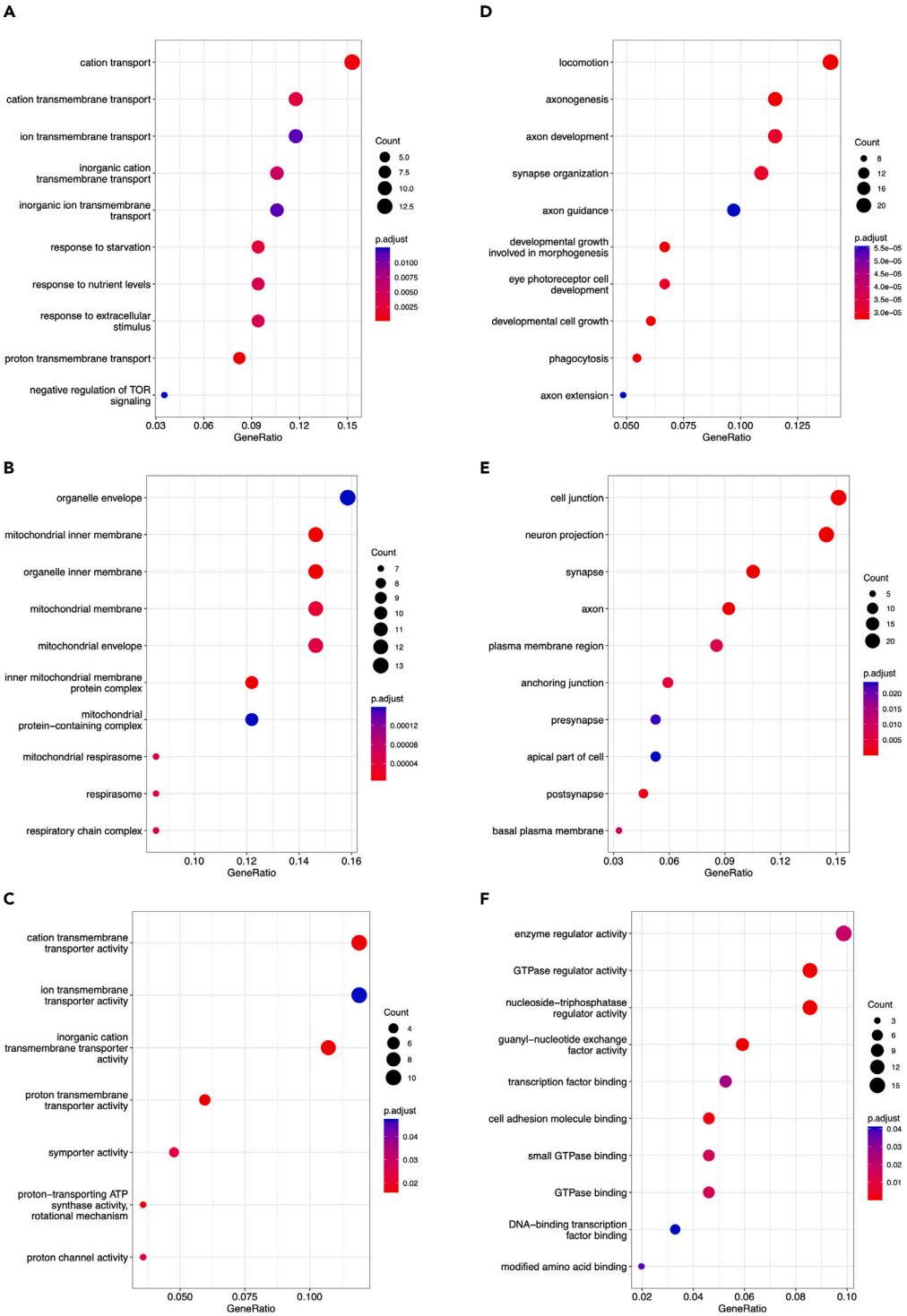

Figure 3. The GO analysis of patterns of differentially expressed genes

(A–F) Differentially expressed genes in pattern 2 (A) biological process analysis, (B) cellular component analysis, (C) molecular function analysis; in pattern 6 (D) biological process analysis, (E) cellular component analysis, (F) molecular function analysis.

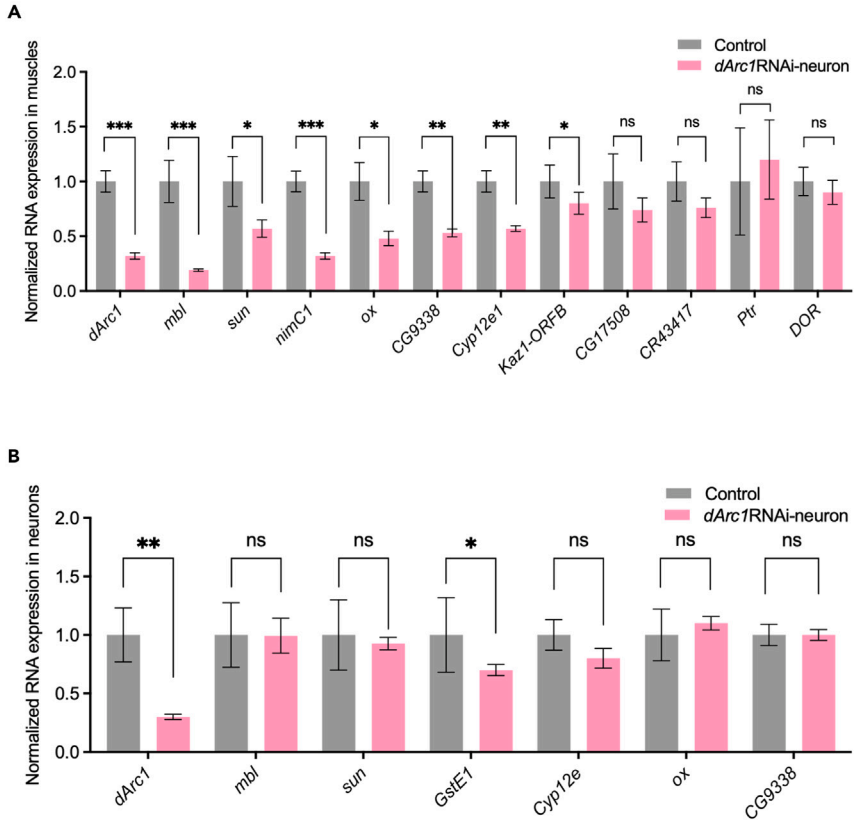

Figure 4. Differentially expressed genes validation

(A) Normalized quantitative PCR confirming some of the target genes in the muscle when *dArc1*RNAi in the neuron. n = 3 biological replicates.

(B) Normalized quantitative PCR confirming most of the target genes in the neuron when *dArc1*RNAi in the neuron. n = 3 biological replicates. Data are presented as mean ± SEM. ns, not significant. *p < 0.05, **p < 0.01, and ***p < 0.001.

RNA immunoprecipitation with dArc1 antibody and RIP-seq analysis

dArc1 protein forms virus-like capsids, binds to RNA transcripts of its own, and transfers across the synapse.[16] In a mammalian synthetic cell culture model, Arc mediates intercellular trafficking of abundant *GFP* mRNA in HEK293 cells.[17] We hypothesized that dArc1 might modify postsynaptic gene expression through its RNA binding function. To determine the RNAs that associate with dArc1, we carried out RNA immunoprecipitation followed by sequencing (RIP-seq). We used a dArc1 antibody or pre-immune serum (non-specific control) to pull down dArc1 protein in homogenates of lysed muscle tissue from wild type flies and then extracted and sequenced the RNAs that co-immunoprecipitated. We performed DEG analysis, to identify enriched genes in pull-down samples with the dArc1 antibody compared to the pre-immune samples. Our analysis of the RIP-seq data revealed that *dArc1* exhibited a significant enrichment in isolated RNA of approximately 5.3-fold (Figures 5A and 5B). We found two genes in our RIP-seq data that had been identified in our RNA-seq data, *mbl* and *nimC1*, which were enriched by 1.68 and 1.64 times, respectively (Figures 5C and S2C).

We then validated these genes by antibody pull-down followed by RT-qPCR. We found that *dArc1* RNA was enriched approximately 2.5 times with the specific antibody, and *mbl* and *nimrodC1* were enriched 1.85 and 3.5 times, respectively. Consistent with our RIP-seq data, we did not find the enrichment of *sun* (Figure 5D). Taken together, our data indicate that dArc1 modifies the expression of different genes pre- and postsynaptically, and a subset of genes that dArc1 affects appears to be through its function in RNA-transport, potentially through direct physical interaction.

mbl, *sun*, and *nimC1* are involved in structural synaptic plasticity at the NMJ

mbl encodes an RNA binding protein which plays a pivotal role in RNA metabolism.[24–26] *mbl* knockdown and overexpression show a similar rough eye phenotype.[39] To examine whether *mbl* is involved in structural synaptic plasticity at the NMJ, we downregulated *mbl* expression separately in pre- and postsynaptic regions by crossing flies having either the motor neuron-specific driver C380-GAL4 or muscle-specific driver C57-GAL4 with two stocks of flies expressing different UAS-*mbl*-RNAi. Disruption of *mbl* in neurons resulted in a drastic reduction in bouton numbers for both RNAi constructs at the third-instar larvae stage (the last stage of larval development before metamorphosis).

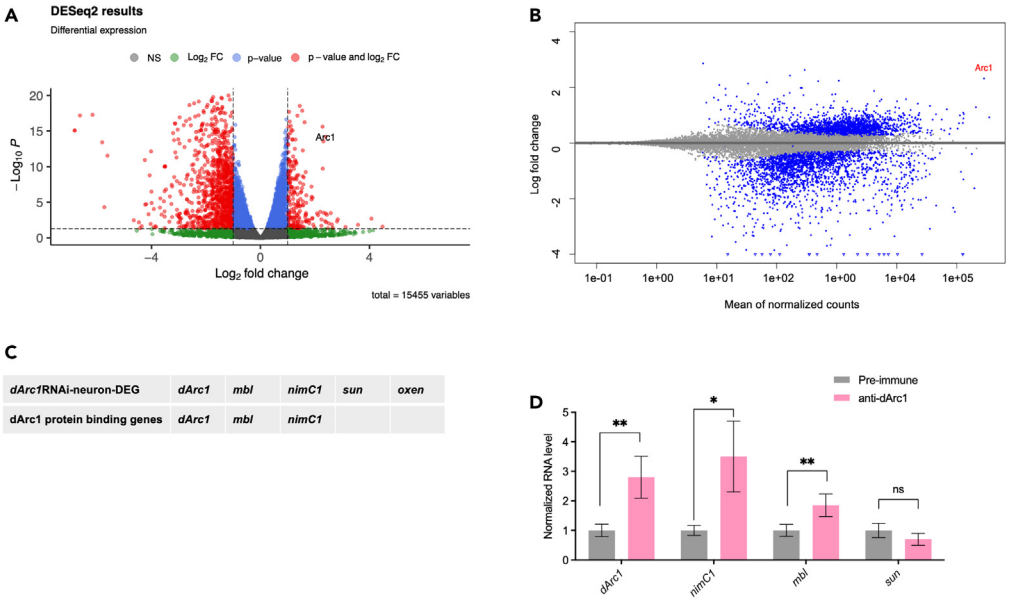

Figure 5. *dArc1*, *mbl* and *nimC1* mRNAs bind to dArc1 protein

(A) Volcano plot of RIP-seq data, where the x axis represents fold change in transcripts from muscle anti-dArc1 immunoprecipitation versus control (a positive score represents enrichment, a negative score represents depletion). The y axis represents statistical confidence for each x axis point.

(B) MA plot of RIP-seq data, where the x axis represents statistical confidence for each y axis point. The y axis represents fold change in transcripts from muscle when *dArc1*RNAi-neuron versus control.

(C) Gene lists from post RNA-seq *dArc1*RNAi-neuron-DEG and dArc1 protein binding genes.

(D) Normalized quantitative PCR confirming *dArc1*, *nimC1* and *mbl* bind to dArc1 protein. n = 3 biological replicates. Data are presented as mean ± SEM. ns, not significant. *p < 0.05, **p < 0.01.

Disrupting *mbl* in the postsynaptic muscle tissue also reduced the number of boutons at this stage for both RNAi constructs (Figures 6A–6G). Immunostaining revealed that mblA protein is mainly expressed in muscle nuclei and at the NMJ (Figure 7A).

sun is a ligand for *mth* proteins, which are located on the neuronal membrane, and together they mediate systemic growth by regulating physiological insulin levels. Importantly, methuselah-like 10 (Mthl10) and its ligands Growth-blocking peptides (Gbps) are required for the increase of cytosolic calcium triggered by wounded cells in *Drosophila*.[32,34,40] To investigate whether *sun* is involved in structural synaptic plasticity, we downregulated *sun* separately in pre- and postsynaptic regions by crossing flies expressing C380-GAL4 or C57-GAL4 drivers with flies expressing UAS-*sun*-RNAi. We found that downregulation of *sun* in the postsynaptic muscle with GAL4 driver C57-GAL4 results in a 40% reduction of bouton numbers, but no significant change in bouton numbers was found when it was disrupted with the motor-neuron-specific driver C380-GAL4 (Figures 6H–6L). The immunostaining result shows that the *sun* protein is broadly expressed in the muscle and highly enriched at the NMJ (Figure 7B).

nimC1 encodes a single-pass transmembrane protein of 90–100 kDa, featuring ten EGF-like repeats (referred to as NIM repeats). It is primarily expressed in phagocytic cells[35] and functions synergistically with the protein Eater to facilitate bacterial phagocytosis.[36] To assess the potential role of *nimC1* in structural synaptic plasticity, we disrupted *nimC1* expression in either pre- or postsynaptic regions by crossing flies expressing the above-mentioned tissue-specific GAL4 drivers with a stock expressing UAS-*nimC1*-RNAi. Our RNA-seq and RT-qPCR analyses revealed that *nimC1* is highly expressed in the muscle, but again was found to be barely expressed in the neuron (Figure S2 A4). Accordingly, we observed a 17% reduction in bouton numbers only when *nimC1* was downregulated in post-synaptic muscle, but no significant reduction was observed when we targeted knockdown of its expression in motor neurons (Figures 6M–6Q). Immunostaining revealed that *nimC1* protein is diffusely expressed in the muscle, but not enriched at the NMJ (Figure 7C).

DISCUSSION

dArc1 mediates structural synaptic plasticity primarily through positive regulation of genes in the muscle

We previously demonstrated that the transfer of dArc1 across the synapse is essential for structural synaptic plasticity.[16] In this study, we found that presynaptic *dArc1* knockdown results in significant changes in gene expression in both pre- and postsynaptic tissues. According to our GO analysis in presynaptic regions, the most impacted pathways were cytoplasmic translation, G protein-coupled receptor signaling pathway, and axon extension. In the postsynaptic regions, the top pathways were cation transmembrane transport, ion transmembrane transport, membrane transporter activity, response to nutrient level, and response to extracellular stimulus.

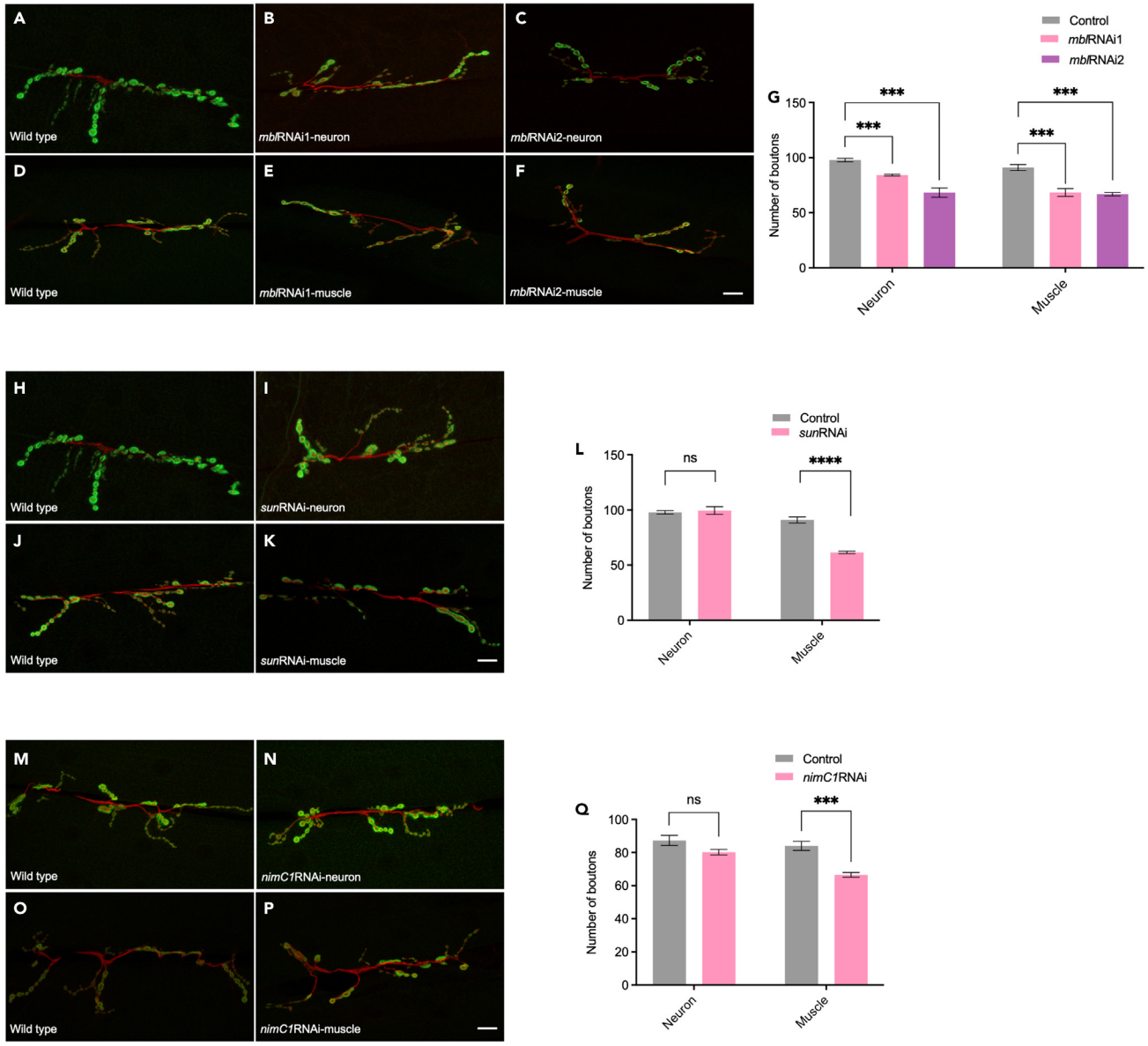

Figure 6. The phenotype of *mbl*, *sun* and *nimC1*

(A–Q) Merged confocal z stacks of NMJ arbors labeled with antibodies against HRP (red) and discs-large (DLG) (green) in (A) C380-Gal4/+ control, (B) *mbl*RNA1i in neuron, (C) *mbl*RNA2i in neuron, (D) C57-Gal4/+ control, (E) *mbl*RNA1i in muscle and (F) *mbl*RNA2i in muscle. (G) Quantification of third-instar larval synaptic boutons in the indicated genotypes and conditions. (H) C380-Gal4/+ control, (I) *sun*RNAi in neuron, (J) C57-Gal4/+ control, (K) *sun*RNAi in muscle. (L) Quantification of third-instar larval synaptic boutons in the indicated genotypes and conditions. (M) C380-Gal4/+ control, (N) *nimC1*RNAi in neuron, (O) C57-Gal4/+ control, (P) *nimC1*RNAi in muscle. (Q) Quantification of third-instar larval synaptic boutons in the indicated genotypes and conditions. Calibration bar is 20 μm.

Considering that dArc1 transfers from pre-to postsynapse along with its own RNA,[16] we attempted to identify dArc1 target genes specific to neurons and muscles, as well as those common to both. To do this, we identified genes in pre- and postsynaptic regions that could be categorized into six distinct expression patterns (Table 1). The DEGs in pattern 2 (ns/-) which included genes known to be involved in structural synaptic plasticity such as *mbl* and *nimC1*, were found to be involved in transmembrane transport, response to nutrient levels, and negative regulation of TOR signaling in biological process analysis. In terms of molecular function, this pattern was associated with cation/ion/inorganic/proton transmembrane transporter activity and symporter activity. These findings support the idea that dArc1 trafficking from pre-to postsynapse with its RNA could affect synaptic plasticity through regulating expression of proteins involved in transport functions and TOR signaling in the postsynaptic tissue, which could be carried out by the DEGs in pattern2 (ns/-). The DEGs in pattern 1 (−/−), which include

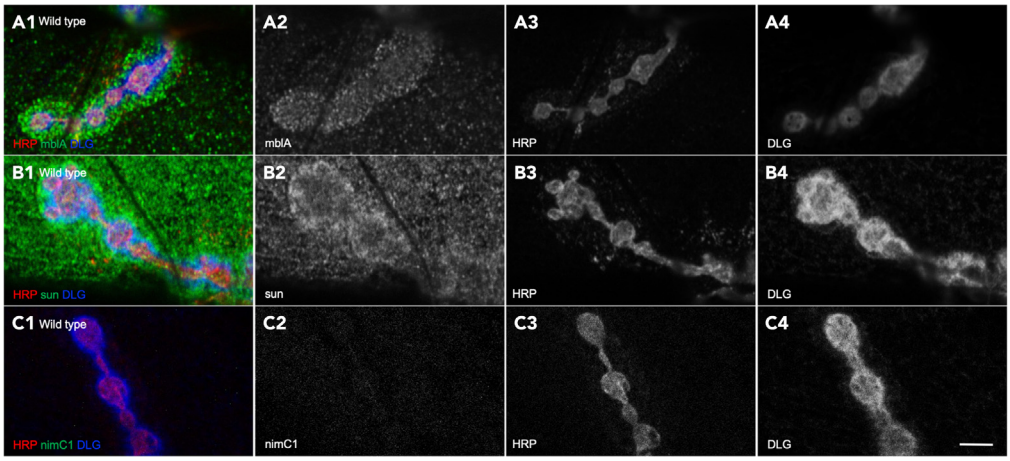

Figure 7. The expression location of *mbl*, *sun*, and *nimC1* protein

(A–C) Merged confocal z stacks of NMJ arbors labeled with antibodies against HRP (red) and discs-large (DLG) (blue) in (A) the expression location of *mbl* protein (green), (B) the expression location of *sun* protein (green), (C) the expression location of *nimC1* protein (green). Calibration bar is 5 μm.

dArc1 and *sun*, were mainly involved in oxidative phosphorylation, respiration, and metabolism in biological processes. These proteins are located on mitochondrial membranes or organelle envelopes in cellular component analysis and exhibited heme binding and G protein-coupled receptor binding in molecular function analysis.

Genes categorized in pattern 6 (+/ns) are involved in locomotion, axonogenesis, axon development, synapse organization, axon guidance, and eye photoreceptor cell development according to the biological process analysis. The proteins encoded by these genes are present in cellular components such as cell junctions, neuron projections, synapses, axons, and presynapses. Molecular function analysis revealed that these DEGs encode proteins that play roles in enzyme regulator activity, GTPase regulator activity, and cell adhesion molecule binding. The genes in pattern 5 (ns/+) did not implicate any specific pathways, which suggests that knockdown of *dArc1* in neurons did not induce a program of gene expression specifically in the muscle that is otherwise repressed. This led us to conclude that in postsynaptic muscles, dArc1 mediates structural synaptic plasticity primarily through positive regulation of gene expression.

dArc1 affects genes expression both pre- and postsynaptically

As an RNA-binding protein, dArc1 binds to its own RNA and transfers across the synapse, and this transfer is necessary for the development of structural synaptic plasticity at the NMJ.[16] We found knockdown of *dArc1* presynaptically reduced the expression of numerous genes in the postsynaptic regions, including its own, by RNA-seq. Subsequently, we conducted RT-qPCR to validate a set of compelling genes, including *mbl*, *sun*, *nimC1*, *ox*, *Kaz1-ORFB*, *CG9338*, *Cyp12e1*, and *DOR*. Considering that dArc1 is an RNA-binding protein, we performed RIP-seq to investigate its RNA cargos. From examining our RNA-seq and RIP-seq datasets, we found that *dArc1* is decreased in the postsynaptic RNA-seq data and enriched in the RIP-seq data, and *mbl* and *nimC1* show this same pattern. We found that knockdown of *mbl* in pre- and postsynaptic regions both caused a reduction of bouton numbers. For *nimC1*, which is mainly expressed in postsynaptic regions, only knockdown in postsynaptic regions caused a reduction in bouton numbers.

mbl is involved in structural synaptic plasticity possibly through alternative splicing

mbl encodes a protein which has been identified as an important player in the regulation of RNA metabolism through its involvement in alternative splicing and localization. In *Drosophila*, *mbl* has been shown to splice the *Dscam2* gene, which is critical for mediating axonal tiling in the visual system. Notably, alternative splicing of exon 10A or 10B in *Dscam2* generates two isoforms that possess distinct extracellular domains with unique biochemical properties. The regulation of this alternative splicing event occurs both spatially and temporally, and *mbl* has been identified as a key mediator of this process.[41–43] In our study, we found *dArc1* knockdown in presynaptic regions, causes the reduction of *mbl* in postsynaptic, but not presynaptic regions, and our RIP-seq data show that *mbl* RNA binds to dArc1 protein. *mbl* knockdown in both pre- and postsynaptic regions cause a reduction of bouton numbers. We hypothesize that the transfer of *mbl* RNA across synapses may be facilitated by the dArc1 protein, leading to alterations in *mbl* RNA and protein levels in postsynaptic regions. These changes subsequently impact the alternative splicing and localization of genes associated with structural synaptic plasticity. However, many aspects of this mechanism have not yet been elucidated, such as identifying the specific target genes of *mbl* and defining how it interacts with other proteins and RNAs. Additionally, it remains to be determined whether dArc1 protein interacts with *mbl* directly or through intermediary components and/or as a complex. The molecular mechanisms of how *mbl* mediates structural synaptic plasticity also need to be further investigated. While there is no data showing that *mbl* is involved in structural synaptic plasticity directly, *mbl* is involved in RNA metabolism through alternative splicing and localization, which implicates it in the regulation of numerous pathways.[24] Identifying

the sets of genes whose regulation and/or splicing are affected when *mbl* is knocked down in the neuron or muscle will be very informative. Identifying the subset of genes that show similar changes with altered *dArc1* expression will help us better understand how these proteins regulate synaptic plasticity.

sun manipulates structural synaptic plasticity by mediating systemic growth

sun encodes a protein which is a ligand for the *mth*-encoded receptor, functioning as a circulating insulinotropic peptide that modulates physiological insulin levels in response to nutrients. This process mediates systemic growth in flies.[34] The *mth*-encoded receptor is specifically expressed at the neuronal membrane at the NMJ. Mutations in the *mth* gene result in a 50% reduction in evoked neurotransmitter release and can only be rescued by presynaptic expression of *mth*.[32] In our RT-QPCR validation dataset, neuronal disruption of *dArc1* causes *sun* expression to be reduced in the postsynaptic (muscle) region, but not changed in the presynaptic (neuron) region. *sun* RNA did not show enrichment in dArc1 pull-down assays. Interestingly, *sun* knockdown in muscle reduced the number of boutons, but knockdown in neurons did not, and sun protein is highly enriched around the NMJ. Based on these findings, we proposed a hypothesis that knockdown of *dArc1* in presynaptic areas results in a reduction of *dArc1* levels in both pre- and postsynaptic regions, leading to decreased *sun* expression in postsynaptic muscles. This, in turn, reduces the activation of the *mth* receptor on the neuronal membrane, resulting in insufficient bouton development at the NMJ. However, further investigation is needed to test this hypothesis, including examining the co-localization of sun ligand and mth receptors at the NMJ, analyzing the impact of *mth* mutations on bouton numbers, and assessing the effect of *sun* overexpression in postsynaptic regions on structural synaptic plasticity development. Defining the interactions of this ligand and receptor family will be crucial to better understand these complex mechanisms. This model system offers great promise for future insights into this area, as studies on how the transfer of *sun* from the muscle to the neuron affects the complex system of synaptic plasticity can be assessed with easy outputs such as the change of bouton numbers.

One challenge in our study is to discern which DEGs are involved in the mechanism of synaptic plasticity and which are differentially regulated as a result of the lack of synaptic plasticity (i.e., distinguishing dysregulation of genes that cause disrupted synaptic plasticity and genes that are dysregulated as an effect of the change in synaptic plasticity). We found that *mbl*, *sun*, and *nimC1* appear to play key roles in structural synaptic plasticity, as their knockdown affects bouton numbers, while disruption of other DEGs such as *Ptr* and *ox* not significantly change structural synaptic plasticity (data not shown). It would be ideal to individually test each of the DEGs that we have identified to more completely examine whether they are involved in synaptic plasticity through ubiquitous or tissue-specific knockdown studies.

In summary, we used *dArc1* knockdown in presynaptic regions as a model, followed by RNA-seq in both pre- and postsynaptic regions and RIP-seq. We found that dArc1 mediates structural synaptic plasticity by regulating the expression of genes involved in diverse cellular processes, including *mbl*, *sun*, and *nimC1*, which play pivotal roles in RNA metabolism, nutrition metabolism, and phagocytosis pathways, respectively. Our results provide new insights into how dArc1 regulates structural synaptic plasticity.

Limitations of the study

Notable limitations of this study include using an invertebrate system at NMJs that may limit how applicable these discoveries are to the vertebrate central nervous system (CNS) where mammalian Arc primarily affects plasticity. We limited our study to bulk RNA sequencing of the *Drosophila* CNS and larval body walls, there are many cell types and neuron types in both tissues that are no doubt diluting out many mRNAs affected by dArc1 mutations, this could be addressed in part by single-cell sequencing. Further, this study did not use an inverse model, specifically a mutation that increased structural synaptic plasticity was not employed to determine which mRNAs were affected in such a paradigm, such a control will go far in validating the mRNAs we identified in *dArc1* mutants. Finally, we did not use *dArc1* mutants that form capsids but do not transfer, which is another powerful control that could have been used to increase confidence in genes identified in this study.

STAR★METHODS

Detailed methods are provided in the online version of this paper and include the following:

- KEY RESOURCES TABLE
- RESOURCE AVAILABILITY
  - Lead contact
  - Materials availability
  - Data and code availability
- EXPERIMENTAL MODEL AND PARTICIPANT DETAILS
  - Flies
- METHOD DETAILS
  - Immunocytochemistry and antibodies
  - Morphometric analysis
  - RT-quantitative PCR
  - RNA IP with RT- quantitative PCR
  - RNA sequencing and RIP-sequencing
- QUANTIFICATION AND STATISTICAL ANALYSIS

SUPPLEMENTAL INFORMATION

Supplemental information can be found online at https://doi.org/10.1016/j.isci.2023.108048.

ACKNOWLEDGMENTS

Thanks to Dr. Leopold and Dr. Ando for the generous gifts of sun and nimC1 antibodies, respectively. We appreciate the Bloomington Drosophila Stock Center, FlyBase, and the Vienna Drosophila Resource Center (VDRC) for invaluable reagents and resources. Thank-you to Alfred Simkin and Gimena Alegre for suggestions and help with data analysis. A special thanks to Erin Piermarini and Angela Jimenez for help with many technical aspects of this project. And also thanks to Dr. Xiang for helpful discussions. This work was supported by NIH grant R01NS112492 to T.T.

AUTHOR CONTRIBUTIONS

Conceptualization, T.T., and C.X.; Methodology, C.X., P.G.M., S.W., A.L., and T.T.; Software, C.X.; Validation, C.X.; Formal Analysis, C.X., P.G.M., S.W., and T.T.; Investigation, C.X., and T.T.; Resources, T.T.; Data Curation, C.X., and T.T.; Writing – Original Draft, C.X. and T.T.; Writing – Review and Editing, C.X. and T.T.; Visualization, C.X.; Supervision, T.T.; Project Administration, C.X., and T.T.; Funding Acquisition, T.T.

DECLARATION OF INTERESTS

The authors declare no competing interests.

INCLUSION AND DIVERSITY

We support inclusive, diverse, and equitable conduct of research.

Received: July 17, 2023
Revised: August 28, 2023
Accepted: September 22, 2023
Published: September 27, 2023

REFERENCES

1. Bosch, M., Castro, J., Saneyoshi, T., Matsuno, H., Sur, M., and Hayashi, Y. (2014). Structural and molecular remodeling of dendritic spine substructures during long-term potentiation. Neuron *82*, 444–459. https://doi.org/10.1016/j.neuron.2014.03.021.
2. Holtmaat, A., and Svoboda, K. (2009). Experience-dependent structural synaptic plasticity in the mammalian brain. Nat. Rev. Neurosci. *10*, 647–658. https://doi.org/10.1038/nrn2699.
3. Kasai, H., Fukuda, M., Watanabe, S., Hayashi-Takagi, A., and Noguchi, J. (2010). Structural dynamics of dendritic spines in memory and cognition. Trends Neurosci. *33*, 121–129. https://doi.org/10.1016/j.tins.2010.01.001.
4. Link, W., Konietzko, U., Kauselmann, G., Krug, M., Schwanke, B., Frey, U., and Kuhl, D. (1995). Somatodendritic expression of an immediate early gene is regulated by synaptic activity. Proc. Natl. Acad. Sci. USA *92*, 5734–5738. https://doi.org/10.1073/pnas.92.12.5734.
5. Lyford, G.L., Yamagata, K., Kaufmann, W.E., Barnes, C.A., Sanders, L.K., Copeland, N.G., Gilbert, D.J., Jenkins, N.A., Lanahan, A.A., and Worley, P.F. (1995). Arc, a growth factor and activity-regulated gene, encodes a novel cytoskeleton-associated protein that is enriched in neuronal dendrites. Neuron *14*, 433–445. https://doi.org/10.1016/0896-6273(95)90299-6.
6. Chowdhury, S., Shepherd, J.D., Okuno, H., Lyford, G., Petralia, R.S., Plath, N., Kuhl, D., Huganir, R.L., and Worley, P.F. (2006). Arc/Arg3.1 interacts with the endocytic machinery to regulate AMPA receptor trafficking. Neuron *52*, 445–459. https://doi.org/10.1016/j.neuron.2006.08.033.
7. Benekareddy, M., Nair, A.R., Dias, B.G., Suri, D., Autry, A.E., Monteggia, L.M., and Vaidya, V.A. (2013). Induction of the plasticity-associated immediate early gene Arc by stress and hallucinogens: role of brain-derived neurotrophic factor. Int. J. Neuropsychopharmacol. *16*, 405–415. https://doi.org/10.1017/S1461145712000168.
8. Steward, O., Farris, S., Pirbhoy, P.S., Darnell, J., and Driesche, S.J.V. (2014). Localization and local translation of Arc/Arg3.1 mRNA at synapses: some observations and paradoxes. Front. Mol. Neurosci. *7*, 101. https://doi.org/10.3389/fnmol.2014.00101.
9. Guzowski, J.F., Lyford, G.L., Stevenson, G.D., Houston, F.P., McGaugh, J.L., Worley, P.F., and Barnes, C.A. (2000). Inhibition of activity-dependent arc protein expression in the rat hippocampus impairs the maintenance of long-term potentiation and the consolidation of long-term memory. J. Neurosci. *20*, 3993–4001. https://doi.org/10.1523/JNEUROSCI.20-11-03993.2000.
10. Shepherd, J.D., and Bear, M.F. (2011). New views of Arc, a master regulator of synaptic plasticity. Nat. Neurosci. *14*, 279–284. https://doi.org/10.1038/nn.2708.
11. Moga, D.E., Calhoun, M.E., Chowdhury, A., Worley, P., Morrison, J.H., and Shapiro, M.L. (2004). Activity-regulated cytoskeletal-associated protein is localized to recently activated excitatory synapses. Neuroscience *125*, 7–11. https://doi.org/10.1016/j.neuroscience.2004.02.004.
12. Fernández, E., Collins, M.O., Frank, R.A.W., Zhu, F., Kopanitsa, M.V., Nithianantharajah, J., Lemprière, S.A., Fricker, D., Elsegood, K.A., McLaughlin, C.L., et al. (2017). Arc Requires PSD95 for Assembly into Postsynaptic Complexes Involved with Neural Dysfunction and Intelligence. Cell Rep. *21*, 679–691. https://doi.org/10.1016/j.celrep.2017.09.045.
13. Zhang, H., and Bramham, C.R. (2021). Arc/Arg3.1 function in long-term synaptic plasticity: Emerging mechanisms and unresolved issues. Eur. J. Neurosci. *54*, 6696–6712. https://doi.org/10.1111/ejn.14958.
14. Bray, N. (2018). Cell biology of the neuron: ARC goes viral. Nat. Rev. Neurosci. *19*, 120–121. https://doi.org/10.1038/nrn.2018.9.
15. Eriksen, M.S., Nikolaienko, O., Hallin, E.I., Grødem, S., Bustad, H.J., Flydal, M.I., O'Connell, R., Hosokawa, T., Lascu, D., Akerkar, S., et al. (2019). Molecular determinants of Arc oligomerization and formation of virus-like capsids. bioRxiv, 667956. https://doi.org/10.1101/667956.
16. Ashley, J., Cordy, B., Lucia, D., Fradkin, L.G., Budnik, V., and Thomson, T. (2018). Retrovirus-like Gag Protein Arc1 Binds RNA and Traffics across Synaptic Boutons. Cell *172*, 262–274.e11. https://doi.org/10.1016/j.cell.2017.12.022.
17. Pastuzyn, E.D., Day, C.E., Kearns, R.B., Kyrke-Smith, M., Taibi, A.V., McCormick, J., Yoder, N., Belnap, D.M., Erlendsson, S., Morado, D.R., et al. (2018). The Neuronal Gene Arc

Encodes a Repurposed Retrotransposon Gag Protein that Mediates Intercellular RNA Transfer. Cell *173*, 275. https://doi.org/10.1016/j.cell.2018.03.024.

18. Cottee, M.A., Letham, S.C., Young, G.R., Stoye, J.P., and Taylor, I.A. (2020). Structure of Drosophila melanogaster ARC1 reveals a repurposed molecule with characteristics of retroviral Gag. Sci. Adv. *6*, eaay6354. https://doi.org/10.1126/sciadv.aay6354.
19. Budnik, V., and Thomson, T. (2020). Structure of an Arc-ane virus-like capsid. Nat. Neurosci. *23*, 153–154. https://doi.org/10.1038/s41593-019-0580-3.
20. Nikolaienko, O., Patil, S., Eriksen, M.S., and Bramham, C.R. (2018). Arc protein: a flexible hub for synaptic plasticity and cognition. Semin. Cell Dev. Biol. *77*, 33–42. https://doi.org/10.1016/j.semcdb.2017.09.006.
21. Myrum, C., Baumann, A., Bustad, H.J., Flydal, M.I., Mariaule, V., Alvira, S., Cuéllar, J., Haavik, J., Soulé, J., Valpuesta, J.M., et al. (2015). Arc is a flexible modular protein capable of reversible self-oligomerization. Biochem. J. *468*, 145–158. https://doi.org/10.1042/BJ20141446.
22. Lee, P.H., Anaya, M., Ladinsky, M.S., Reitsma, J.M., and Zinn, K. (2022). An extracellular vesicle targeting ligand that binds to Arc proteins and facilitates Arc transport *in vivo*. Elife. https://doi.org/10.1101/2022.09.06.506798.
23. Budnik, V., Koh, Y.H., Guan, B., Hartmann, B., Hough, C., Woods, D., and Gorczyca, M. (1996). Regulation of synapse structure and function by the Drosophila tumor suppressor gene dlg. Neuron *17*, 627–640.
24. Wang, E.T., Cody, N.A.L., Jog, S., Biancolella, M., Wang, T.T., Treacy, D.J., Luo, S., Schroth, G.P., Housman, D.E., Reddy, S., et al. (2012). Transcriptome-wide regulation of pre-mRNA splicing and mRNA localization by muscleblind proteins. Cell *150*, 710–724. https://doi.org/10.1016/j.cell.2012.06.041.
25. Pamudurti, N.R., Patop, I.L., Krishnamoorthy, A., Bartok, O., Maya, R., Lerner, N., Ashwal-Fluss, R., Konakondla, J.V.V., Beatus, T., and Kadener, S. (2022). circMbl functions in cis and in trans to regulate gene expression and physiology in a tissue-specific fashion. Cell Rep. *39*, 110740. https://doi.org/10.1016/j.celrep.2022.110740.
26. Ashwal-Fluss, R., Meyer, M., Pamudurti, N.R., Ivanov, A., Bartok, O., Hanan, M., Evantal, N., Memczak, S., Rajewsky, N., and Kadener, S. (2014). circRNA biogenesis competes with pre-mRNA splicing. Mol. Cell *56*, 55–66. https://doi.org/10.1016/j.molcel.2014.08.019.
27. Begemann, G., Paricio, N., Artero, R., Kiss, I., Pérez-Alonso, M., and Mlodzik, M. (1997). muscleblind, a gene required for photoreceptor differentiation in Drosophila, encodes novel nuclear Cys3His-type zinc-finger-containing proteins. Development *124*, 4321–4331.
28. Llamusi, B., Bargiela, A., Fernandez-Costa, J.M., Garcia-Lopez, A., Klima, R., Feiguin, F., and Artero, R. (2013). Muscleblind, BSF and TBPH are mislocalized in the muscle sarcomere of a Drosophila myotonic dystrophy model. Dis. Model. Mech. *6*, 184–196. https://doi.org/10.1242/dmm.009563.
29. Rogalska, Z., and Sobczak, K. (2022). Sustainable recovery of MBNL activity in autoregulatory feedback loop in myotonic dystrophy. Mol. Ther. Nucleic Acids *30*, 438–448. https://doi.org/10.1016/j.omtn.2022.10.023.
30. Kanadia, R.N., Johnstone, K.A., Mankodi, A., Lungu, C., Thornton, C.A., Esson, D., Timmers, A.M., Hauswirth, W.W., and Swanson, M.S. (2003). A muscleblind knockout model for myotonic dystrophy. Science *302*, 1978–1980. https://doi.org/10.1126/science.1088583.
31. Charizanis, K., Lee, K.Y., Batra, R., Goodwin, M., Zhang, C., Yuan, Y., Shiue, L., Cline, M., Scotti, M.M., Xia, G., et al. (2012). Muscleblind-like 2-mediated alternative splicing in the developing brain and dysregulation in myotonic dystrophy. Neuron *75*, 437–450. https://doi.org/10.1016/j.neuron.2012.05.029.
32. Song, W., Ranjan, R., Dawson-Scully, K., Bronk, P., Marin, L., Seroude, L., Lin, Y.J., Nie, Z., Atwood, H.L., Benzer, S., and Zinsmaier, K.E. (2002). Presynaptic regulation of neurotransmission in Drosophila by the g protein-coupled receptor methuselah. Neuron *36*, 105–119. https://doi.org/10.1016/s0896-6273(02)00932-7.
33. Cvejic, S., Zhu, Z., Felice, S.J., Berman, Y., and Huang, X.Y. (2004). The endogenous ligand Stunted of the GPCR Methuselah extends lifespan in Drosophila. Nat. Cell Biol. *6*, 540–546. https://doi.org/10.1038/ncb1133.
34. Delanoue, R., Meschi, E., Agrawal, N., Mauri, A., Tsatskis, Y., McNeill, H., and Léopold, P. (2016). Drosophila insulin release is triggered by adipose Stunted ligand to brain Methuselah receptor. Science *353*, 1553–1556. https://doi.org/10.1126/science.aaf8430.
35. Kurucz, E., Márkus, R., Zsámboki, J., Folkl-Medzihradszky, K., Darula, Z., Vilmos, P., Udvardy, A., Krausz, I., Lukacsovich, T., Gateff, E., et al. (2007). Nimrod, a putative phagocytosis receptor with EGF repeats in Drosophila plasmatocytes. Curr. Biol. *17*, 649–654. https://doi.org/10.1016/j.cub.2007.02.041.
36. Melcarne, C., Ramond, E., Dudzic, J., Bretscher, A.J., Kurucz, É., Andó, I., and Lemaitre, B. (2019). Two Nimrod receptors, NimC1 and Eater, synergistically contribute to bacterial phagocytosis in Drosophila melanogaster. FEBS J. *286*, 2670–2691. https://doi.org/10.1111/febs.14857.
37. Frolov, M.V., Benevolenskaya, E.V., and Birchler, J.A. (2000). The oxen gene of Drosophila encodes a homolog of subunit 9 of yeast ubiquinol-cytochrome c oxidoreductase complex: evidence for modulation of gene expression in response to mitochondrial activity. Genetics *156*, 1727–1736. https://doi.org/10.1093/genetics/156.4.1727.
38. Fernandes, A.C., Uytterhoeven, V., Kuenen, S., Wang, Y.C., Slabbaert, J.R., Swerts, J., Kasprowicz, J., Aerts, S., and Verstreken, P. (2014). Reduced synaptic vesicle protein degradation at lysosomes curbs TBC1D24/sky-induced neurodegeneration. J. Cell Biol. *207*, 453–462. https://doi.org/10.1083/jcb.201406026.
39. García-Casado, M.Z., Artero, R.D., Paricio, N., Terol, J., and Pérez-Alonso, M. (2002). Generation of GAL4-responsive muscleblind constructs. Genesis *34*, 111–114. https://doi.org/10.1002/gene.10147.
40. O'Connor, J.T., Stevens, A.C., Shannon, E.K., Akbar, F.B., LaFever, K.S., Narayanan, N.P., Gailey, C.D., Hutson, M.S., and Page-McCaw, A. (2021). Proteolytic activation of Growth-blocking peptides triggers calcium responses through the GPCR Mthl10 during epithelial wound detection. Dev. Cell *56*, 2160–2175.e5. https://doi.org/10.1016/j.devcel.2021.06.020.
41. Millard, S.S., Flanagan, J.J., Pappu, K.S., Wu, W., and Zipursky, S.L. (2007). Dscam2 mediates axonal tiling in the Drosophila visual system. Nature *447*, 720–724. https://doi.org/10.1038/nature05855.
42. Millard, S.S., Lu, Z., Zipursky, S.L., and Meinertzhagen, I.A. (2010). Drosophila dscam proteins regulate postsynaptic specificity at multiple-contact synapses. Neuron *67*, 761–768. https://doi.org/10.1016/j.neuron.2010.08.030.
43. Li, J.S.S., and Millard, S.S. (2019). Deterministic splicing of Dscam2 is regulated by Muscleblind. Sci. Adv. *5*, eaav1678. https://doi.org/10.1126/sciadv.aav1678.
44. Budnik, V. (1996). Synapse maturation and structural plasticity at Drosophila neuromuscular junctions. Curr. Opin. Neurobiol. *6*, 858–867.
45. Stewart, B.A., Atwood, H.L., Renger, J.J., Wang, J., and Wu, C.F. (1994). Improved stability of Drosophila larval neuromuscular preparations in haemolymph-like physiological solutions. J. Comp. Physiol. *175*, 179–191.
46. Koh, Y.H., Popova, E., Thomas, U., Griffith, L.C., and Budnik, V. (1999). Regulation of DLG localization at synapses by CaMKII-dependent phosphorylation. Cell *98*, 353–363.
47. Bolger, A.M., Lohse, M., and Usadel, B. (2014). Trimmomatic: a flexible trimmer for Illumina sequence data. Bioinformatics *30*, 2114–2120. https://doi.org/10.1093/bioinformatics/btu170.
48. Dobin, A., Davis, C.A., Schlesinger, F., Drenkow, J., Zaleski, C., Jha, S., Batut, P., Chaisson, M., and Gingeras, T.R. (2013). STAR: ultrafast universal RNA-seq aligner. Bioinformatics *29*, 15–21. https://doi.org/10.1093/bioinformatics/bts635.
49. Jin, Y., Tam, O.H., Paniagua, E., and Hammell, M. (2015). TEtranscripts: a package for including transposable elements in differential expression analysis of RNA-seq datasets. Bioinformatics *31*, 3593–3599. https://doi.org/10.1093/bioinformatics/btv422.
50. Love, M.I., Huber, W., and Anders, S. (2014). Moderated estimation of fold change and dispersion for RNA-seq data with DESeq2. Genome Biol. *15*, 550. https://doi.org/10.1186/s13059-014-0550-8.
51. Yu, G., Wang, L.G., Han, Y., and He, Q.Y. (2012). clusterProfiler: an R package for comparing biological themes among gene clusters. OMICS *16*, 284–287. https://doi.org/10.1089/omi.2011.0118.

STAR★METHODS

KEY RESOURCES TABLE

REAGENT or RESOURCE	SOURCE	IDENTIFIER
Antibodies		
Rabbit anti-DLG	Koh et al., 1999	N/A
Mouse anti-DLG	Koh et al., 1999	N/A
Rabbit anti-mblA	This study	N/A
Guinea pig anti-sun	Delanoue et al., 2016	N/A
Mouse anti-nimC1	Kurucz et al., 2007	N/A
DyLight-594-conjugated goat anti-HRP	Jackson ImmunoResearch	Cat#123515021
DyLight-488-conjugated goat anti-rabbit	ThermoScientific	Cat#35553
anti-Mouse IgG Alexa Flour 488	Jackson ImmunoResearch	Cat#115545166
DyLight-649-conjugated donkey anti-rabbit	Jackson ImmunoResearch	Cat#711495152
anti-Guinea pig IgG DyLight 649	Jackson ImmunoResearch	Cat#706495148
Chemicals, peptides, and recombinant proteins		
Formamide	ThermFisher	Cat#AM9342
RNeasy Micro Kit	QIAGEN	Cat#74004
RNeasy Mini Kit	QIAGEN	Cat#74104
Next Ultra directional RNA library prep kit for Illumina sequencing	NEB	Cat#E7420S
Streptavidin magnetic beads	ThermoFisher	Cat#88816
RIPA buffer	Abcam	Cat#ab156034
TurboDNase	ThermoFisher	Cat#AM2238
SuperScript™ IV First-Strand Synthesis System	ThermoFisher	Cat#18091200
Sybr green master mix	Applied Biosystems	Cat#A25741
Pierce™ Protein A/G Magnetic Beads	ThermoFisher	Cat#88803
Deposited data		
RNA-seq and RIP-seq data	this paper	PRJNA948042
Experimental models: organisms/strains		
C380-Gal4	Budnik, 1996	N/A
C57-Gal4	Budnik, 1996	N/A
UAS-*dArc1*-RNAi	Ashley et al., 2018	N/A
CantonS (CS)	Bloomington *Drosophila* stock center	BDSC:64349
UAS-*mbl*-RNAi1	Vienna *Drosophila* Resource Center	v28732
UAS-*mbl*-RNAi2	Vienna *Drosophila* Resource Center	v105486
UAS-*mblA*	García-Casado	N/A
UAS-*mblC*	García-Casado	N/A
UAS-*sun*-RNAi	Vienna *Drosophila* Resource Center	v23685
UAS-*nimC1*-RNAi	Vienna *Drosophila* Resource Center	v1031
Oligonucleotides		
dArc1 (F-ACTTCTCCGCTTGCACACAC and R-TCCTTGTATGTCTCGATGTTGC)	Integrated DNA Technologies	Custom made
18S (F-CTGAGAAACGGCTACCACATC and R-ACCAGACTTGCCCTCCAAT)	Integrated DNA Technologies	Custom made

(*Continued on next page*)

Continued

REAGENT or RESOURCE	SOURCE	IDENTIFIER
mbl (F-CACAATTCTGCAAAACGCCG and R-CACATACACGTGCACTCGC)	Integrated DNA Technologies	Custom made
sun (F-ATGACTGCCTGGAGAGCTG and R-GTGAACTTCACATGGCTCGC)	Integrated DNA Technologies	Custom made
nimC1 (F-GAGACTGCCTACAGGACCGTA and R-GCAGAATCCATGTTGAGGACAC)	Integrated DNA Technologies	Custom made
ox (F-CAACACCCTGTTCAAGCGC and R-ATGCCCTCGAAAATCGCAAC)	Integrated DNA Technologies	Custom made
CG9338 (F-ATCTTGGCTCTCACCGTCTTG and R-CGAGGCTACTGTCTGACTTGA)	Integrated DNA Technologies	Custom made
Cyp12e1 (F-AACGCAGTGGAACGCAAATAA and R-TCCCGGAATATCAGCATAAGGT)	Integrated DNA Technologies	Custom made
Kaz1-ORFB (F-TAGCGAAAACCCCTGGTTGAG and GCATGAATGGAAACAGGCGAAA)	Integrated DNA Technologies	Custom made
CG17508 (F-CGTTTGCGGTGCTGAAAGG and R-GGGGAATTGAGGCTTCATTCAC)	Integrated DNA Technologies	Custom made
CR43417 (F-CCGGGCGGATATCTGGGAAA and R-CCATCCACGATGACTGGGCT)	Integrated DNA Technologies	Custom made
Ptr (F-GCCTGCTACGGAATCACCCA and R-GTATGCTCCAGGGTGCTGGT)	Integrated DNA Technologies	Custom made
DOR (F-CTTGATCTCGGGGTGTCGAC and R-TTCAACTGTACGGCCGCAT)	Integrated DNA Technologies	Custom made
Software and algorithms		
Volocity Software (version 6.3.1)	PerkinElmer	http://cellularimaging.perkinelmer.com/downloads/
DeSeq2	Love et al., 2014	https://bioconductor.org/packages/release/bioc/html/DESeq2.html
TEtranscripts	Jin et al., 2015	https://github.com/mhammell-laboratory/TEtranscripts
Trimmomatic	Bolger et al., 2014	https://github.com/usadellab/Trimmomatic
STAR	Dobin et al., 2013	https://github.com/alexdobin/STAR/releases
clusterProfiler	Yu et al., 2012	https://bioconductor.org/packages/release/bioc/html/clusterProfiler.html
Alliance	N/A	https://www.alliancegenome.org/

RESOURCE AVAILABILITY

Lead contact

Further information and requests for resources and reagents should be directed to Travis Thomson (travis.thomson@umassmed.edu).

Materials availability

No reagents were generated in the study.

Data and code availability

All data is represented in the main paper and/or supplemental information. The software, algorithms and codes which are used in the paper are referred to in the key resources table.

The present study did not produce novel code. Additional information on the reported data is available from the lead contact upon request. Any additional information required to reanalyze the data reported in this paper is available from the lead contact upon request.

RNA-seq data (RNA sequencing, Illumina, transcriptome) has been deposited at NCBI (PRJNA948042) and are publicly available as of the date of publication. Accession numbers are listed in the key resources table. All other data is available upon request to the lead contact.

EXPERIMENTAL MODEL AND PARTICIPANT DETAILS

Flies

The following fly lines were used: the wild type strain, CantonS (CS) (64349, Bloomington Drosophila stock center, BDSC), C380-Gal4 and C57-Gal4,[44] UAS-*dArc1*-RNAi,[16] UAS-*mbl*-RNAi1 (v28732, Vienna Drosophila Resource Center), UAS-*mbl*-RNAi2 (v 105486, Vienna Drosophila Resource Center), UAS-*mblA* and UAS-*mblC*,[39] UAS-*sun*-RNAi (v23685, Vienna Drosophila Resource Center), UAS-*nimC1*-RNAi (v1031, Vienna Drosophila Resource Center). Female 3rd Instar larvae were dissected for NMJ preparations to ensure consistency. The flies were reared on molasses-based standard food, either at 25°C (for most crosses) or at 29°C (for RNAi crosses).

METHOD DETAILS

Immunocytochemistry and antibodies

Third instar larval body wall muscles were dissected in low calcium HL3 saline (0.1 mM Calcium[45]) and fixed in 4% paraformaldehyde in 0.1 M phosphate buffer. The fixed larvae were then washed and permeabilized in phosphate-buffered saline with Triton X-100 (PBT; 0.1 M phosphate buffer; 0.2% (v/v) Triton X-100) and incubated with primary antibody overnight at 4°C. Subsequently, the samples were washed three times with PBT and incubated in secondary antibodies for 2 hours at room temperature. After incubation with secondary antibodies, the samples were again washed three times with PBT and mounted in Vectashield (Vector Laboratories). The primary antibodies used were rabbit anti-DLG at 1:40,000 dilution,[46] mouse anti-DLG at 1:200 dilution, guinea pig anti-sun at 1:50 dilution, rabbit anti-MblA at 1:500 dilution, and rabbit anti-nimC1 at 1:200 dilution. The secondary antibodies were DyLight-conjugated secondary antibodies from Jackson ImmunoResearch (DyLight-594-conjugated goat anti-HRP, DyLight-488-conjugated anti-mouse or anti-rabbit) at 1:200 dilution, and anti-Guinea Pig IgG DyLight-649 at 1:200 dilution.

Morphometric analysis

Images shown in the figures were captured under identical settings for both the control and experimental groups. The imaging process was conducted simultaneously on a Zeiss LSM 800 confocal microscope system and Zen software (Zeiss Microscopy Inc) equipped with a Zeiss 63X Plan-Apochromat 1.40 NA DIC M27 oil immersion objective and a Zeiss 40X Plan-Apochromat 1.30 NA DIC (UV) VIS-IR M27 oil immersion objective was used for acquisition. To quantify the number of synaptic boutons, the preparations were labeled with both presynaptic marker (anti-HRP) and postsynaptic marker (anti-Dlg), and the boutons were counted.

RT-quantitative PCR

For each genotype, either five larval body wall muscles or 10 brains were homogenized in RLT buffer (QIAGEN) with 20 μl 2 M dithiothreitol (DTT) per 1 ml RLT buffer pre-added, and RNA was extracted using the RNeasy microKit (QIAGEN). DNase (TurboDNase (ThermoFisher) was applied to RNA samples from different genotypes, and 100 ng of RNA was reverse transcribed into cDNA using a Superscript IV kit (ThermoFisher). The RT-quantitative PCRs were carried out in triplicate in a 96-well plate (BioRad) using a CFX96 system (BioRad). A Sybr green master mix (ThermoFisher) was used with gene-specific primer sets for *dArc1*, *mbl*, *sun*, *nimC1*, *ox*, *CG9338*, *Cyp12e1*, *Kaz1-ORFB*, *CG17508*, *CR43417*, *Ptr*, *DOR*, and 18S rRNA (all sequences are listed in the Key Resources Table). All transcript levels were normalized to the *18S* transcript level.

RNA IP with RT- quantitative PCR

For each biological replicate, 10 larval body wall muscles were homogenized in RIPA buffer (Abcam) from wild type animals. The resulting supernatants were cleared using magnetic beads (Pierce) and pre-immune serum, and then incubated with either an anti-dArc1 antibody or an equal amount of pre-immune serum. The samples were incubated with serum and magnetic beads overnight and washed six times with RIPA buffer. RNA was finally eluted from the beads with RLT buffer (QIAGEN) and purified using the RNeasy micro kit (QIAGEN). Briefly, wild type flies were homogenized in RIPA buffer (Abcam) supplemented with RNase inhibitor (100 U/ml), EDTA (5 mM), DTT (0.5 mM), and protease inhibitor, and homogenized with an electric homogenizer. The blade was rinsed twice with another 450 μl lysis buffer, and the homogenate was given constant agitation for 30 minutes at 4°C. The resulting supernatants were cleared using magnetic beads for 20 minutes, followed by rabbit pre-immune serum for 1 hour at 4°C. The samples were then incubated with rabbit serum or dArc1 antibody (5–10 μg input) overnight, followed by incubation with magnetic beads for 2 hours and then washed six times with RIPA buffer. RNAs were eluted from the beads with RLT buffer (QIAGEN) containing 20 μl of 2 M dithiothreitol (DTT) added per 1 ml of RLT buffer, and RNA was extracted using the RNeasy microKit (QIAGEN). The quantitative RT-PCR step was the same as described above.

RNA sequencing and RIP-sequencing

RNA concentration and integrity were assessed using the Qubit 4 Fluorometer (Thermo Fisher Scientific) and 2100 Bioanalyzer (Agilent), respectively. RNA libraries were prepared using the NEBNext® Ultra™ II Directional RNA Library Prep Kit for Illumina® kit without any modifications. Each library had an input of approximately 500 ng total RNA, and a total of nine PCR cycles were used for library amplification. The concentration and quality of libraries were assessed using the Qubit 4 Fluorometer (Thermo Fisher Scientific) and 2100 Bioanalyzer

(Agilent), respectively. The libraries were normalized to 20 nM and pooled, then further normalized to a final concentration of 5 nM, loaded onto the NextSeq500/550 High Output Kit v2.5(150 Cycles) chip (Illumina), and sequenced on the NextSeq550 (Illumina).

Reads were sorted by barcode for each library and adapter sequences were removed using Trimmomatic.[47] The reads were then mapped to the *Drosophila* genome using STAR,[48] and the gene expressions were counted using TEtranscripts.[49] DEGs were identified using DeSeq2[50](Love et al., 2014). GO analysis was performed using clusterProfiler.[51]

QUANTIFICATION AND STATISTICAL ANALYSIS

Statistical analyses were performed using GraphPad Prism software 9 (GraphPad Software Inc., San Diego, CA). All experiments were performed at least three times independently. For comparison of a single experimental sample with control, Student's t-test was used. For the comparison of multiple experimental groups, a one-way analysis of variance (ANOVA) was used followed by Tukey's post hoc test. In all figures, ns, not significant, * $p<0.05$, ** $p<0.01$, and *** $p<0.001$. Data in bar graphs are presented as mean $\pm$ SEM.